

**SYNTHESIS OF CE DOPED ZNO NANOPARTICLES  
USING LASER ASSISTED CHEMICAL BATH  
TECHNIQUE FOR PHOTOCATALYTIC  
IMPROVEMENT**

**AL RIKABY AWRAS HAMEED AJIL**

**UNIVERSITI SAINS MALAYSIA**

**2025**

**SYNTHESIS OF CE DOPED ZNO NANOPARTICLES  
USING LASER ASSISTED CHEMICAL BATH  
TECHNIQUE FOR PHOTOCATALYTIC  
IMPROVEMENT**

**by**

**AL RIKABY AWRAS HAMEED AJIL**

**Thesis submitted in fulfilment of the requirements  
for the degree of  
Doctor of Philosophy**

**September 2025**

## ACKNOWLEDGEMENT

I endured easy and difficult, good and thought-provoking times in the course of this research; hence I would like to thank Allah Almighty for His mercy, and bounty and for granting me health, patience, and the willpower to satisfactorily carry out this research with this incredible journey successfully. My gratitude and appreciation also go to my main supervisor Associate Prof. Dr. Yam Fong Kwong for his support, patience, immense assistance, encouragement, and inspiring guidance in ensuring the completion of my research perfectly. My sincere indebtedness, gratefulness, and deepest thanks go to my Co-supervisor, Associate Prof. Dr. Naser M. Ahmed for his thoughtful insights, motivation, and guidance throughout my study.

I am grateful for the love and encouragement my beloved parents have always provided during every endeavor. Also, none of this would have been possible without the lasting love, consideration, and support of my husband Zeyad Mustafa. I also use this medium to appreciate my sweet sister and brothers for their continual support and prayers. I am forever grateful for their patience, concern, care, love, financial, and moral support.

My gratitude also goes to the staff of the School of Physics, NOR lab, Solid State Lab, and the FESEM lab staff, and also the staff of the School of Chemistry USM, for their enormous assistance. Much of this work would be incomplete without their technical support. My appreciation and gratitude to all my friends and colleagues, thank you for your assistance and support.

## TABLE OF CONTENTS

<b>ACKNOWLEDGEMENT.....</b>	<b>ii</b>
<b>TABLE OF CONTENTS.....</b>	<b>iii</b>
<b>LIST OF TABLES.....</b>	<b>viii</b>
<b>LIST OF FIGURES.....</b>	<b>x</b>
<b>LIST OF SYMBOLS.....</b>	<b>xv</b>
<b>LIST OF ABBREVIATIONS.....</b>	<b>xvii</b>
<b>LIST OF APPENDICES.....</b>	<b>xix</b>
<b>ABSTRAK.....</b>	<b>xx</b>
<b>ABSTRACT.....</b>	<b>xxi</b>
<b>CHAPTER 1 INTROUDICTION .....</b>	<b>1</b>
1.1 Background of the study.....	1
1.2 Problem statement.....	3
1.3 Research objectives.....	6
1.4 Novelties of the study.....	6
1.5 Scope of the study.....	7
1.6 Thesis outline.....	8
<b>CHAPTER 2 LITERATURE REVIEW.....</b>	<b>10</b>
2.1 Introduction .....	10
2.2 Dye pollutants .....	11
2.2.1 The Methyl Orange (MO) dye .....	11
2.2.2 Dye removal techniques.....	12
2.3 Metal oxide Semiconductors for photodegradation .....	12
2.4 The fundamental properties of ZnO.....	13

2.4.1	Optical properties of ZnO.....	14
2.4.2	ZnO nanoparticles properties.....	15
2.5	ZnO NPs modification by doping .....	16
2.6	RE metal modification.....	17
2.7	The fundamental properties of Ce (Cerium) metal.....	20
2.8	The fundamental properties of photocatalyst.....	21
2.9	Advanced Oxidation Process of pollutant degradation .....	22
2.10	Photocatalytic evaluation under light.....	25
2.10.1	The Effects of light wavelength and intensity on Photodegradation.....	26
2.11	Adsorption and degradation.....	27
2.11.1	The degradation removal efficiency.....	28
2.11.2	Photocatalysis kinetics studies.....	28
2.11.3	Isotherm studies of MO dye molecules for photocatalytic system.....	29
2.12	The laser light.....	30
2.13	Synthesising nanoparticle with Laser light technique.....	30
2.13.1	Synthesis the ZnO and Ce-doped ZnO nanoparticles with IR laser.....	32
2.13.2	Synthesis the ZnO and Ce-doped ZnO of nanoparticles with blue laser.....	34
2.14	Laser photothermal effect.....	35
2.15	Laser decomposition .....	37
2.16	The effects of CW laser wavelength and power on nanoparticle synthesis.....	38
<b>CHAPTER 3 METHODOLOGY.....</b>		<b>42</b>
3.1	Introduction.....	42
3.2	Cleaning tools.....	44

3.3	Preparing undoped ZnO and Ce-doped ZnO solutions.....	45
3.4	Photocatalyst preparation.....	46
3.5	Thermal annealing.....	46
3.6	Characterization tools.....	47
3.6.1	Field Emission Scanning Electron Microscopy and Energy dispersive X-ray .....	47
3.6.2	X-ray Diffractometer .....	49
3.6.3	UV-Visible Spectrophotometer .....	51
3.7	Preparation MO dye aqueous solution.....	52
3.8	Photocatalytic activity.....	53
3.8.1	The experiments setup of MO dye degradation.....	54
3.8.1(a)	Dark condition.....	54
3.8.1(b)	In the presence of light.....	54
<b>CHAPTER 4 RESULTS AND DISCUSSION.....</b>		<b>56</b>
4.1	Introduction.....	56
4.2	Characterization .....	56
4.2.1	The UV-visible spectroscopy and optical properties.....	56
4.2.1(a)	The IRL and BL synthesised undoped ZnO Photocatalyst.....	56
4.2.1(b)	The IRL 1%-4%Ce-doped ZnO NPs.....	59
4.2.1(c)	The BL 1%-4%Ce-doped ZnO NPs.....	64
4.2.1(d)	The effects of Ce dopant content and laser radiation on optical properties.....	66
4.2.2	XRD assessments .....	68
4.2.2(a)	The undoped ZnO photocatalysts.....	68
4.2.2(b)	The 1 wt% Ce-doped ZnO NPs.....	70
4.2.2(c)	The 2 wt% Ce-doped ZnO NPs.....	72

4.2.2(d)	The 3 wt% Ce-doped ZnO NPs.....	74
4.2.2(e)	The 4 wt% Ce-doped ZnO NPs.....	75
4.2.2(f)	Crystallite size and strain analyses.....	76
4.2.2(g)	The effects of Ce content and laser radiation on the XRD results.....	79
4.2.3	FESEM observations.....	80
4.2.3(a)	The undoped ZnO photocatalysts.....	80
4.2.3(b)	The IRL synthesised 1 wt%–4 wt% Ce-doped ZnO photocatalysts.....	81
4.2.3(c)	The BL synthesised 1 wt%–4 wt% Ce-doped ZnO photocatalysts.....	83
4.2.4	EDX evaluations.....	85
4.2.4(a)	The undoped ZnO photocatalysts.....	85
4.2.4(b)	The IRL synthesised 1 wt%–4 wt% Ce-doped ZnO Photocatalyst.....	86
4.2.4(c)	The BL synthesised 1 wt%–4 wt% Ce-doped ZnO Photocatalyst.....	87
4.2.4(d)	The influences of Ce incorporation and laser radiation assessed via FESEM and EDX.....	88
4.3	Photocatalytic Activities of the Manufactured Photocatalyst Under UV and Sunlight.....	90
4.3.1	The MO dye adsorption analyses in the dark.....	90
4.3.2	The photocatalytic degradation of MO dye with the undoped ZnO NPs powders.....	91
4.3.3	The photocatalytic degradation of MO dye utilising the IRL 1 wt%–4 wt% Ce-doped ZnO NPs powders.....	92
4.3.4	The photocatalytic degradation of MO dye utilising the BL 1 wt%–4 wt% Ce-doped ZnO NPs powders.....	95
4.3.5	The MO dye degradation removal efficiency.....	97
4.3.5(a)	The undoped ZnO NPs photocatalysts.....	97

4.3.5(b)	The IRL 1 wt%–4 wt% Ce-doped ZnO photocatalysts.....	99
4.3.5(c)	The BL 1 wt%–4 wt% Ce-doped ZnO photocatalysts.....	101
4.3.6	Kinetics studies of photocatalysis under light exposure.....	103
4.3.6(a)	The undoped ZnO NPs photocatalysts.....	103
4.3.6(b)	The IRL 1 wt%–4 wt% Ce-doped ZnO photocatalysts.....	104
4.3.6(c)	The BL 1 wt%–4 wt% Ce-doped ZnO photocatalysts.....	107
4.3.7	The dye molecule isotherms under light exposure .....	109
4.3.7(a)	The undoped ZnO NPs photocatalysts.....	109
4.3.7(b)	The IRL 1 wt%–4 wt% Ce-doped ZnO photocatalysts.....	110
4.3.7(c)	The BL 1 wt%–4 wt% Ce-doped ZnO Photocatalysts.....	111
4.4	The proposed photodegradation and adsorption mechanisms .....	113
4.5	The effects of Ce dopant on photocatalytic activity performance.....	116
4.6	The effects of light wavelength and intensity on photodegradation efficiency.....	119
4.7	The influence of laser wavelength and power on the synthesised nanoparticles.....	120
4.8	The MO dye photodegradation performance comparison between the synthesised photocatalysts and other studies .....	121
<b>CHAPTER 5 CONCLUSIONS AND RECOMMENDATIONS.....</b>		<b>123</b>
5.1	Conclusions.....	123
5.2	Recommendations.....	124
<b>REFERENCES.....</b>		<b>125</b>
<b>APPENDICES</b>		
<b>LIST OF PUBLICATIONS</b>		

## LIST OF TABLES

		<b>Page</b>
Table 2.1	The fundamental properties of ZnO semiconductors.....	13
Table 2.2	A summary of selected recent reports doping ZnO by variety of metal dopants for efficient photocatalyst in the degradation of different pollutant.....	17
Table 2.3	The fundamental properties of Cerium metal.....	21
Table 2.4	A review of CW high power lasers in nanomaterial Synthesis.....	41
Table 4.1	The lattice parameters, <i>c/a</i> ratio, <i>d</i> -spacing, Zn-O bond length ( <i>L</i> ), crystalline size ( <i>D</i> ), and strain ( $\epsilon$ ) of the IRL and BL undoped ZnO samples .....	69
Table 4.2	The lattice parameters, <i>c/a</i> ratio, <i>d</i> -spacing, Zn-O bond length ( <i>L</i> ), crystalline size ( <i>D</i> ), and strain ( $\epsilon$ ) of the IRL and BL Ce/ZnO samples.....	77
Table 4.3	The ImageJ software results of the IRL and BL ZnO NPs.....	81
Table 4.4	The IRL 1 wt%–4 wt% Ce-ZnO NPs measurements via ImageJ.....	83
Table 4.5	The BL 1 wt%–4 wt% Ce-ZnO NPs sizes via ImageJ software.....	85
Table 4.6	The degradation rates of the undoped BL and IRL ZnO NPs.....	92
Table 4.7	The MO degradation rate percentages of the IRL 1 wt%-4 wt% Ce/ZnO NPs.....	94
Table 4.8	The 1 wt%–4 wt% Ce/ZnO NPs (BL) degradation rate percentages.....	95
Table 4.9	The rate constants ( <i>k</i> ) with linear regression coefficients ( $R^2$ ) of the pseudo-first and -second orders for the IRL and BL ZnO NPs under UV and sunlight.....	104

Table 4.10	The $k$ and $R^2$ of pseudo-first and second orders of the IRL 1 wt%–4 wt% Ce/ZnO NPs under UV and sunlight.....	106
Table 4.11	The pseudo-first and second orders $k$ and $R^2$ of the BL 1 wt%–4 wt% Ce/ZnO NPs under UV and sunlight.....	109
Table 4.12	The IRL and BL ZnO NPs adsorption capacities.....	110
Table 4.13	The adsorption capacities ( $q_e$ and $q_t$ ) of the IRL 1 wt%–4 wt% Ce/ZnO NPs.....	111
Table 4.14	The adsorption capacities ( $q_e$ and $q_t$ ) of the BL 1 wt%–4 wt% Ce/ZnO NPs.....	112
Table 4.15	The comparative survey results of MO dye solution removal through UV and sunlight through photocatalysis with Ce/ZnO photocatalysts synthesised via different methods.....	122

## LIST OF FIGURES

	<b>Page</b>
Figure 1.1	The schematic presentation of of MO dye adsorption in the dark and photodegradation mechanism by Ce/ZnO NPs photocatalyst under light (Note: Modified from [23]).....3
Figure 2.1	The hexagonal wurtzite structure of ZnO.....14
Figure 2.2	The schematic presentation of the photocatalytic mechanism and degradation process.....24
Figure 2.3	The schematic illustration of a standard IR laser system.....32
Figure 2.4	The schematic representation of the experimental setup for the IR laser.....33
Figure 2.5	The schematic illustration of a standard blue laser system.....34
Figure 2.6	The schematic representation of the experimental blue laser setup.....35
Figure 2.7	The schematic illustration of photothermal effects and VB (solid lines) and CB energy levels (dotted lines).....36
Figure 2.8	The schematic diagram of nanoparticle formation (Note: Modified from [148]).....38
Figure 3.1	The photocatalyst powder synthesis flow chart.....43
Figure 3.2	The schematic representation of the experimental setup for the IR laser.....44
Figure 3.3	The ceramic boat.....45
Figure 3.4	The thermal annealing tube of a blue furnace (Lenton VTF/12/60/700).....47
Figure 3.5	The FEI Nova NanoSEM FESEM system.....48
Figure 3.6	The high-resolution XRD system.....49

Figure 3.7	The Carry series UV-Vis-NIR DRS spectrophotometer.....	51
Figure 3.8	The MO powder and sample solution.....	53
Figure 3.9	The MO dye solution photodegradation setup under (a) UV flashlight source and (b) sunlight.....	54
Figure 3.10	The MO dye absorption curve (a.u.) vs wavelength (nm) (Note: Created by author).....	55
Figure 3.11	(a) The absorbance curves of five different concentrations (a.u.) of MO dye against wavelength (nm) and (b) the calibration line of the absorbance (a.u.) vs concentration (ppm) of MO dye (Note: Created by author).....	55
Figure 4.1	The optical absorbance spectra of the pure ZnO (Blue) and IRL (Black) and BL (Orange) undoped ZnO NPs from 200 nm to 800 nm.....	57
Figure 4.2	The $(\alpha E)^2$ versus E evaluations during $E_g$ value estimations for pure ZnO (Blue) and undoped IRL (Black) and BL (Orange) ZnO NPs.....	59
Figure 4.3	The undoped and Ce-doped ZnO samples irradiated with IR laser.....	60
Figure 4.4	The UV-VIS spectra of the 1 wt%–4 wt% Ce-doped ZnO nanoparticles synthesised through IR laser from 200 nm to 800 nm.....	60
Figure 4.5	The UV-VIS spectra and $(\alpha E)^2$ versus E (inset) for estimating the $E_g$ values of the 1 wt%–4 wt% Ce-doped ZnO nanoparticles synthesized by IRL.....	61
Figure 4.6	The undoped and Ce-doped ZnO samples irradiated with Blue laser.....	64
Figure 4.7	The UV-VIS spectra of the 1 wt%–4 wt% Ce-doped ZnO NPs synthesised with Blue laser from 200 nm to 800 nm.....	64

Figure 4.8	The UV-VIS spectra and $(\alpha E)^2$ versus E (inset) assessment for estimating the $E_g$ value of the 1 wt%–4 wt% Ce-doped ZnO nanoparticles synthesised with BL.....	65
Figure 4.9	The XRD pattern of the undoped ZnO NPs synthesised with (a) IRL and (b) with BL.....	68
Figure 4.10	The XRD pattern comparison between 1 wt%–4 wt% Ce/ZnO NPs synthesised with (a) IRL and (b) BL, respectively ( <i>Note: The blue planes refer to hcp, red represents fcc, and green is bco.</i> ) .....	70
Figure 4.11	The FESEM images of the (a) IRL and (b) BL undoped ZnO nanoparticle powder at 4 $\mu$ m and 500 nm (inset) scales.....	80
Figure 4.12	The IRL (a) 1 wt%, (b) 2 wt%, (c) 3 wt%, and (d) 4 wt% Ce-doped ZnO NPs powder FESEM images at 5 $\mu$ m and 500 nm (inset) scales.....	82
Figure 4.13	The BL (a) 1 wt%, (b) 2 wt%, (c) 3 wt%, and (d) 4 wt% Ce-doped ZnO NPs powder FESEM images at 5 $\mu$ m and 500 nm (inset) scales.....	84
Figure 4.14	The undoped (a) IRL and (b) BL ZnO NPs EDX spectra.....	86
Figure 4.15	The IRL (a) 1 wt%, (b) 2 wt%, (c) 3 wt%, and (d) 4 wt% Ce-doped ZnO NPs EDX spectra.....	87
Figure 4.16	The BL (a) 1 wt%, (b) 2 wt%, (c) 3 wt%, and (d) 4 wt% Ce-doped ZnO NPs EDX spectra.....	88
Figure 4.17	The MO solution degradation absorption curves with IRL and BL ZnO NPs under UV and sunlight.....	91
Figure 4.18	The MO dye degradation absorption curves in the presence of IRL 1 wt%–4 wt% Ce/ZnO NPs under UV and sunlight.....	93

Figure 4.19	The MO solution degradation with 1 wt%–4 wt% Ce/ZnO NPs (BL) absorption curves under UV and sunlight.....	95
Figure 4.20	The IRL and BL ZnO NPs MO dye removal efficiencies in the dark and under UV and sunlight at 120 min Ultimate time .....	98
Figure 4.21	The relative MO molecule concentration photodegradation with the IRL and BL ZnO NPs efficiency in the dark and under UV and sunlight at 120 min Ultimate time.....	98
Figure 4.22	The MO dye removal efficiency by the IRL 1wt%–4 wt% Ce/ZnO NPs in the dark and under UV and sunlight at 120 min Ultimate time.....	99
Figure 4.23	The relative MO molecule concentration photodegradation efficiency with the 1 wt%–4 wt% Ce/ZnO NPs (IRL) in the dark and under UV and sunlight at 120 min Ultimate time.....	101
Figure 4.24	The MO dye removal efficiency by the BL 1wt%–4 wt% Ce/ZnO NPs in the dark and under UV and sunlight at 120 min Ultimate time.....	102
Figure 4.25	The relative MO molecule concentration photodegradation efficiency with the 1 wt%–4 wt% Ce/ZnO NPs (BL) in the dark and under UV and sunlight at 120 min Ultimate time.....	102
Figure 4.26	The first- and second-order reaction kinetics for the degradation of MO by the IRL and BL ZnO NPs under UV and sunlight.....	104
Figure 4.27	The first-order MO degradation reaction kinetics by the IRL 1wt%–4 wt% Ce/ZnO NPs under UV and sunlight.....	105

Figure 4.28	The second-order MO degradation reaction kinetics of the IRL 1 wt%–4 wt% Ce/ZnO NPs samples under UV and sunlight.....	105
Figure 4.29	The MO degradation first-order reaction kinetics by the BL 1 wt%–4 wt% Ce/ZnO NPs under UV and sunlight.....	107
Figure 4.30	The BL 1 wt%–4 wt% Ce/ZnO NPs MO degradation second-order reaction kinetics under UV and sunlight.....	108
Figure 4.31	The MO dye adsorption capacity with time of the IRL and BL ZnO NPs under UV and sunlight (right) and in the dark (left).....	109
Figure 4.32	The MO dye adsorption capacity with time of the IRL 1 wt%–4 wt% Ce/ZnO NPs under UV and sunlight (right) and in the dark (left).....	111
Figure 4.33	The BL 1 wt%–4 wt% Ce/ZnO NPs MO dye adsorption capacity with time under UV and sunlight (right) and in the dark (left).....	112
Figure 4.34	The dye degradation mechanisms on the Ce/ZnO NPs surface under light.....	114
Figure 4.35	The dye adsorption on the surface of doped Ce/ZnO NPs photocatalyst mechanisms in the dark.....	115

## LIST OF SYMBOLS

$A$	Absorption
$\text{\AA}$	Angstrom
$c$	Speed of light.
$^{\circ}\text{C}$	Degree celsius
$C_o$	Concentration of MO dye without photocatalyst
$C_t$	Concentration of MO dye with photocatalyst
$D$	Crystallite size
$d$	Inter planer spacing
$\bar{e}/h^+$	Electron-hole pair
$e_{cb}^-$	Conduction band electron
eV	Electron volt
$E_g$	Band gap energy
gm	gram
h	Hour
$h$	Planck's constant
$h_{vb}^+$	Valence band hole
$h\nu$	Photon energy (E)
J	Joule
K	Kelvin
$k_1$	Rate constants of Pseudos' first order reaction
$k_2$	Rate constants of Pseudos' second order reaction
kV	Kilo volt
L	Liter

$M$	Mass
M	Molarity
mA	Milli ampere
mg	Milli gram
Min	Minute
ml	Milliliter
mol	Mole
nm	nanometer
$q_e$	Amount of MO dye at equilibrium
$q_t$	Amount of MO dye at any time
$R$	Correlation factor
$R^2$	Regression coefficients
s	Second
t	Time
T	Temperature
$V$	Volume
W	Watt
wt%	Weight percent
$\alpha$	Absorption coefficient
$\beta$	Full Width at Half Maximum
$\varepsilon$	Strain
$\theta$	Bragg angle
$\lambda$	Wavelength
$\mu$	Micrometre

## LIST OF ABBREVIATIONS

AOP	Advanced Oxidation Process
AZ	Atrazine pollutant
bco	Base Centered Orthorhombic
BL	Visible range (Blue colour beam)
BLACBS	Blue Laser-Assisted Chemical Bath Synthesis
CB	Conduction Band
CIP	Ciprofloxacin
CW	Continuous Wave
DI	De-Ionized Water
DRS	Diffuse Reflectance Spectroscopy
3D	Three Dimensions
EDX	Energy dispersive X-ray
EIS	Electrochemical Impedance Spectroscopy
fcc	face-centered cubic
FESEM	Field Emission Scanning Electron Microscopy
FWHM	Full Width at Half Maximum
FTIR	Fourier-Transform Infrared
hcp	hexagonal closely packed
IR	Invisible infrared range radiation
IRLACBS	Infrared Laser-Assisted Chemical Bath Synthesis
LACBS	Laser-Assisted Chemical Bath Synthesis
MB	Methylene Blue
MO	Methyl Orange

NIR	Near Infrared region
NPs	Nanoparticles
PC	Personal Computer
ppm	part per million
RE	Rare Earth
RhB	Rhodamine B
RR180	Reactive Red 180
ROS	Reactive Oxygen Species
rpm	rotation per minute
SAS	Supercritical Anti Solvent
SCS	Self-Combustion Synthesis
TEM	Transmission Electron Microscope
UV	Ultra-Violet wavelength region in the spectrum
UV-VIS	UV-Visible Spectrophotometer
VB	Valance Band
wt%	Weight (molecular weight) Percent
XRD	X-ray Diffractometer
XPS	X-ray Photoelectron Spectroscopy

## **LIST OF APPENDICES**

Appendix A Figure A-1

Appendix B Figure B-1

Figure B-2

Figure B-3

Appendix C Proofreading and translations certificates

# **SINTESIS NANOPARTIKEL ZNO TERDOP CE MENGGUNAKAN TEKNIK RENDAMAN KIMIA TERBANTU LASER UNTUK PENAMBAHBAIKAN FOTOKATALITIK**

## **ABSTRAK**

Metil Jingga (MO) ialah pewarna sintetik toksik yang lazim digunakan dalam pewarnaan. Pelepasan pewarna ini ke dalam sungai nyata sekali mencabar. Penghasilan nano-fotopemangkin yang kos efektif dan mesra alam untuk rawatan air semakin mendapat perhatian. Kajian ini memberi tumpuan kepada sintesis terdop dengan nanozarah ZnO terdop Cerium (Ce) daripada larutan melalui gelombang berterusan (CW) dan laser kuasa tinggi yang mengurangkan jurang jalur ZnO yang tidak didop untuk meningkatkan penuaian cahaya. IRL merupakan laser gas karbon dioksida (CO<sub>2</sub>) pada daerah inframerah dengan panjang gelombang 10.6 µm. Sementara itu, BL dilengkapi dengan laser semikonduktor diod pada daerah biru dengan panjang gelombang 450 nm. Laser inframerah dan laser biru digunakan melalui Rendaman Kimia Berbantu Laser (IRLACBS) dan sintesis (BLACBS). Selepas itu, kesan fototerma dan penguraian laser menghasilkan nanozarah tanpa bahan tambah kimia dan keperluan tenaga rendah. Kaedah tersebut memberikan ketepatan, keberkesanan kos, efisiennya, dan manfaat alam sekitar berbanding dengan teknik konvensional. Data UV-VIS, FESEM, EDX, XRD, dan ImageJ mengesahkan pengedopan Ce ke dalam matriks ZnO serta pembentukan nanozarah sfera tiga dimensi (3D). Efisiennya tertinggi bagi fotopemangkin yang disintesis dalam mendegradasikan pewarna MO dinilai dengan kadar hasil optimum ketara dicatatkan pada 95% dan pemalar kadar tindak balas kinetik  $k_1 = 0.0271 \text{ min}^{-1}$  bagi ZnO terdop 1%brt. Ce (IRL) di bawah cahaya matahari, manakala 93%, dan  $k_1 = 0.02203 \text{ min}^{-1}$  bagi ZnO terdop 1%brt. Ce (BL) di bawah cahaya UV dalam tempoh (20–90) minit.

# **SYNTHESIS OF CE DOPED ZNO NANOPARTICLES USING LASER ASSISTED CHEMICAL BATH TECHNIQUE FOR PHOTOCATALYTIC IMPROVEMENT**

## **ABSTRACT**

Methyl Orange (MO) is a toxic synthetic dye commonly employed during dyeing that released into rivers water is significantly challenging. Fabricating eco-friendly and cost-effective nano-photocatalyst for water treatment is gaining interest. The current study focused on synthesising Cerium (Ce)-doped ZnO nanoparticles (NPs) of solution via continuous wave (CW) and high-power lasers that reduces the bandgap of undoped ZnO to improve light harvesting. The IRL is a carbon dioxide (CO<sub>2</sub>)-gas laser at the infrared region with a 10.6 μm wavelength. Meanwhile, BL is equipped with a diode semiconductor laser, at the blue region of 450 nm. The Infrared and blue lasers are used through Laser-Assisted Chemical Bath (IRLACBS) and (BLACBS) syntheses. Subsequently, the photothermal effect and laser decomposition, resulted in NPs without chemical additives and low-energy requirements. The methods offer precision, cost-effectiveness, efficiency, and environmental benefits over conventional techniques. The UV-VIS, FESEM, EDX, XRD, and ImageJ data validated of the doping Ce into the ZnO matrix and the formation of three-dimensional (3D) spherical NPs. The highest efficiencies of the synthesised photocatalysts in degrading MO dye was assessed with notable optimal results were recorded at 95% and kinetic reaction rate constant  $k_1 = 0.0271 \text{ min}^{-1}$  for 1 wt% Ce-doped ZnO (IRL) under sunlight, while 93% and  $k_1 = 0.02203 \text{ min}^{-1}$  for 1 wt% Ce-doped ZnO (BL) under UV light within (20-90) minutes. The products had dual functions: photocatalyst-adsorbent under light and dark. The synthesised photocatalysts offer eco-friendly, efficient economic, and functional environmental remediation.

## CHAPTER 1

### INTRODUCTION

#### 1.1 Background of the study

Humans require water for daily life, a predominant element of health, cleanliness, and productivity. Researchers are aiming to discover novel, efficient, and low-cost strategies for treating polluted water due to lack of access to clean water worldwide [1][2]. Accordingly, developing effective wastewater treatments from industrial processes is a global objective, specifically treating persistent organic pollutants. Most dyes are not eliminated in wastewater treatment plants, ending in surface and groundwater [3]. Methyl orange (MO) is a synthetic dye commonly utilised during dyeing. The substance is also the most frequently employed synthetic dye in several fields, including textiles, paper, plastics, and cosmetics, released to rivers, lakes, and oceans is considerably challenging.

The need for green and eco-friendly synthesis techniques that offer the potential to produce nanostructures with desired properties [4]. Nanostructures can be synthesised via different physical and chemical methods, such as hydrothermal, sol-gel, and co-precipitation [5]. Laser allows the substantially synthesis of nanoparticles with controllable features. Applying CW, high-powered lasers through Laser-Assisted Chemical Bath syntheses (LACBS) as decomposition technique in solutions. The approach consumes low energy, cost, and time, offers ease of employment, and does not necessitate a vacuum system and additive chemicals [6][7][8].

Advanced oxidation processes (AOPs) are effective approaches for treating wastewater through photocatalysis [9]. Metal oxide-based photocatalysis is an advanced approach significantly affecting the field of water purification [10]. The candidate in the photocatalytic process is Zinc oxide (ZnO) has demonstrated superior

chemically and thermally suitability, non-toxic, wide direct bandgap, and binding energy (60 meV) [11]. The considerable surface area of the substance offers excellent ultraviolet (UV) light harvesting properties, and reactive species generation (ROS) enabling effective employment in wastewater remediation [12].

Metal oxide semiconductors have been modified with metal dopants, including silver (Ag), aluminium (Al), copper (Cu), and other. The approach improves the photocatalytic performance of the semiconductors through enhanced contaminant degradation through electron transfers to ZnO conduction band (CB) [13][14]. Cerium (Ce), a rare earth element, has received attention as a promising dopant due to its inexpensiveness, low toxicity, and remediation benefits. Moreover, the substance possesses photogenerated charge carrier trapping capabilities, 4f orbital availability, and Ce-O ionic bonding [15][16]. The Ce ion also decrease the electron-hole pair recombination rates and narrow the band gap by generating additional energy levels [17][18].

Typically, the metal dopants added to the ZnO matrix reside at substitution or interstitial sites. The substance expands absorption range and improves light utilisation of photocatalysts [15]. The reports investigated the influences of doping with Ce on the optical, structural, and electronic characteristics of the rods. The recycling data indicated that ZnO:Ce rods are a reliable solar-light photocatalyst. Consequently, Ce-doped ZnO offers sustainability as its solar-to-chemical conversion properties presents an ideal strategy with vast potential to solve environmental issues regarding photogenerated ( $e^-/h^+$ ) pair separations and participates in redox reactions on photocatalyst surfaces during MO dye light degradation [1][2][19].

The mechanism of MO dye degradation through AOP in the presence of Ce-doped ZnO under light was determined in the current study. If a Ce-doped ZnO NPs

photocatalyst that has achieved adsorption-desorption equilibrium in the dark is excited by light, an electron is excited from its valence band (VB) to an empty conduction band (CB), yielding an  $e^-/h^+$  pair that participated in redox reactions via produce hydroxyl radicals, powerful oxidising agents that attack the pollutants adsorbed on the Ce/ZnO surface (Figure 1.1), producing carbon dioxide ( $CO_2$ ) and water ( $H_2O$ ) [20][21][22].

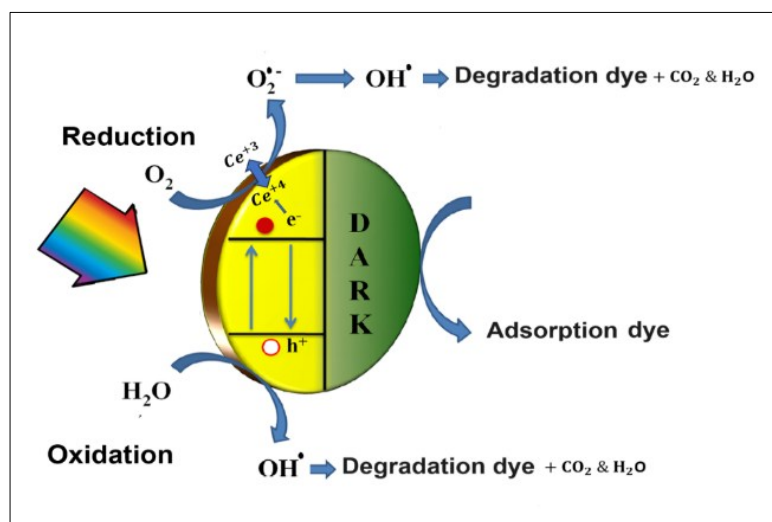


Figure 1.1 The schematic presentation of MO dye adsorption in the dark and photodegradation mechanism by Ce/ZnO NPs photocatalyst under light (Note: Modified from [23])

## 1.2 Problem statement

Methyl orange (MO) is the most often employed synthetic dye in various industries. Nonetheless, the substance is considerably toxic. Consequently, efficient and cost-effective synthesis methods for producing efficient photocatalysts are necessary. The photocatalysts should be capable of breaking down pollutants through photodegradation in water that making it safe for human consumption [2][24].

The Existing literature largely focuses on traditional approaches of Ce/ZnO nanomaterials were synthesised with different fabrication methods, such as simple hydrothermal method [20], chemical precipitation [25], and combustion [26]. The using of these traditional methods for nanostructures production are affected by several parameters, including pH, temperature, solute concentration, reaction time, and drying.

Furthermore, the inability to regulate the growth, due synthesizing under high temperature and pressure conditions or numerous steps and long heating and cooling periods, often produce NPs with large particle sizes and poor reproducibility [27][28][29].

Laser light is the sole energy source for precursor molecule dissociation, nucleation, and assembly into various nanostructures. CW high-power lasers technology significantly presents a promising alternative to traditional chemical synthesis enabling rapid, additive-free, and reproducible nanoparticle production, influence the final product morphology, structure, and high-quality NPs [28]. In this study, A CW 60-watt and 20-watt, the Infrared and blue lasers are employed in Laser-Assisted Chemical Bath IRLACBS and BLACBS techniques respectively, were suggested for applied as a decomposition targeted solution of rapidly growth efficient NPs. Moreover, laser technique may allow feature regulation, required low energy, cost-effective and easy to use in room conditions, did not require a vacuum system and additive chemicals. Therefore, they are less toxic, economical, and effective, and there is an urgent need for such methods for NPs synthesis [6][7][8].

The ZnO nanostructures have gained interest due to their diverse morphologies, availability, non-toxicity, light sensitivity, and low processing costs. The substance also possesses notable thermal chemical stability and response speed, which are advantageous for water treatment purposes [30][31][32]. Furthermore, its nano structure enhances ZnO physical and optical properties [30][31][32]. The ZnO NPs photocatalyst has a wide UV illumination activation bandgap, encompassing 3%–5% of sunlight, presenting a disadvantage [33]. Furthermore, its rapid photogenerated ( $e^-/h^+$ ) pair recombination negatively affects the ZnO NP photocatalytic efficiency [34][35].

Consequently, ZnO NPs are doped with metal ions, such as rare earth (RE) metal elements, has received great attention due to its atypical properties arising from the availability of the 4f shell [36][37]. Doped ZnO nano-photocatalyst have high surface area that can produce reactive oxygen species (ROS) in the presence of light [11][35]. Also demonstrated photogenerated charge carrier trapping abilities, thus inhibiting electron-hole ( $\bar{e}/h^+$ ) pair recombination [19][30][38]. Consequently, the photocatalysts exhibit increased light response in the visible region, versatility, and efficiency in facilitating dye degradation without requiring additional reagents [17][22][39]. Suggesting doping with Ce ions may improve ZnO performance from diminished crystallite size and bandgap, and may enhance photodegradation [14].

A new major innovative challenge in environmental photocatalysis is achieving efficient degradation under light and dark conditions to ensure complementary pollutant degradation, which is poorly documented. Thus, there is a pressing need to develop and investigate Ce-ZnO NPs that rapidly deliver high-efficiency solar light utilization and sustained activity even in the absence of light, thereby making the technology viable for environmental remediation. Direct sunlight exposure can be extensively exploited for pollutant degradation in outdoor environments. The abundant, sustainable, and continuous irradiation that solar energy offers is an economical and environmentally friendly light source [40][41]. Also, Photocatalytic activities with a flashlight in the UV wavelength range to establish the applications in the indoor environment. Consequently, the photocatalytic activities of the synthesizing nanoparticles need to be evaluated on MO dye degradation performance. The removal efficiency, kinetics, and isotherm performance of the nanomaterials.

### **1.3 Research objectives**

The current study aimed to synthesise the photocatalysts undoped and 3D spherical Ce-doped ZnO NPs utilising high power and CW lasers through IRLACBS and BLACBS. The photocatalysts are applied for degradation MO dye under dark and light conditions. The objectives of this study are as follows:

- (i) To synthesise spherical 3D nanoparticles via high-power and CW IRLACBS and BLACBS photolysis techniques in solution for procuring efficient NPs with controllable growth, without additional reagents or systems.
- (ii) To assess the influence of Ce doping into ZnO photocatalytic performance with reduced bandgap and size of the synthesised nanoparticles in rapidly degrading MO dye under UV (396 nm) flashlight and solar light.
- (iii) To evaluate the dual-functionality under light and dark effectiveness, efficiencies, kinetics, and isotherms analyses of the photocatalyst in MO dye degradation with solar light and UV flashlight as green, economical, and real-world environmental remediation.

### **1.4 Novelties of the study**

The novelties offered by the proposed methodology are listed as follows:

- (i) Fabricating significantly uniform 3D spherical Ce-doped ZnO nanoparticles through high-powered 60- and 20-watt IRACBS and BLACBS approaches in solution with laser photolysis without requiring additional reagents and systems.
- (ii) Synthesising photocatalysts with small size of considerably small bandgap notably of efficient and rapid MO dye photodegradation capabilities in the dark and under UV and sunlight.
- (iii) Applying IR and Blue LACBS to produce dual functionality solar and UV photocatalysts as a significantly cost-effective and efficient method for degrading MO

dye, especially under solar radiation, considering the substantial attention it has garnered globally.

### **1.5 Scope of the study**

The current study focused on fabricating undoped and Ce-doped ZnO NPs with LACBS via laser decomposition. The use of CW and high-power IRACBS and BLACBS for nanoparticle growth is advantageous due to its efficiency and the comparison the product powders.

In this study, photocatalyst nanopowders are applied to degrade MO dye during water treatments and was evaluated for efficiency. Furthermore, the effects of Ce doping content at different concentration percentages on degradation activity under UV and sunlight were compared. Several characterisation equipment, including XRD, SEM, EDX, UV-VIS DRS, and ImageJ software were employed to analyse the properties of the synthesised nanoparticles.

In the present study, the MO dye rapid and dual functionality degradation abilities of the synthesised nanomaterial were evaluated under dark and light. Finally, the MO dye photodegradation reaction of degradation were established through efficiency, kinetic, and isotherm assessments.

The degradation mechanisms of the undoped and doped ZnO photocatalysts were also established. Moreover, the influences of Ce doping, laser wavelength, power, and irradiation time, on the synthesised photocatalysts were assessed. The photocatalytic activities of the manufactured nanoparticles were compared to Ce-doped ZnO NPs prepared through different methods.

### **1.6 Thesis outline**

This thesis is divided into five chapters. Chapter One (Introduction) briefly describes MO dye pollutants and photocatalysis in wastewater treatment. The problem

statements on issues requiring investigations are also included in the chapter. An objectives and novelties of the present study of the IRLACBS and BLACBS methods of synthesis photocatalyst for degrading MO dye under dark and light conditions and evaluation under UV flashlight and sunlight. Chapter 1 also discusses the scope of the study and thesis organisation.

Chapter Two, the Literature Review section, discusses previous reports on photocatalysis. The section of the thesis provides a brief explanation of ZnO fundamental and optical properties. The basic principles and fundamentals of photocatalysis are also included. Furthermore, fundamentals information regarding the RE Ce also modifications and photocatalytic evaluation under light and removal analyses assessments are provided. Finally, type of lasers, photothermal effects, laser decomposition, and the influence of laser parameters on the photocatalytic activities are discussed.

The experimental segment of this study is covered in Chapter Three (Materials and Methods) of this thesis. The chapter describes the materials, chemical reagents, and the research methodology applied in the present study. The thermal annealing and characterization tools employed are also included. The experimental setup, photocatalyst characterisations, performance evaluation. Furthermore, flowcharts demonstrating the synthesis and photocatalytic mechanisms are included.

The findings and discussions of the results are detailed in Chapter Four (Results and Discussion). Outlines of the characterisation, optical properties, structures, compositions, and morphology, Ce doping content effects on the photocatalytic degradation performances under light and dark conditions. The photocatalytic activities under UV and sunlight, adsorption under dark, removal efficiency, kinetic, and isotherm analyses. Furthermore, the MO photocatalytic degradation mechanisms

of dual functionality undoped and Ce-doped ZnO NPs under light and dark conditions were established. The effects of laser parameters and Ce doping on the MO photocatalytic degradation and comparison with findings reported by other studies.

Chapter Five (Conclusions and Recommendations) summarises the findings documented in Chapter Four. The section of the thesis also includes conclusions and recommendations for future studies. Furthermore, the chapter discusses several improvements applicable to the present study.

## CHAPTER 2

### LITERATURE REVIEW

#### 2.1 Introduction

A significant focus has been placed on addressing industrial pollution. The harmful products released into water damage the environment, aquatic life, human health, and the economy. The potential of semiconductor oxides in mitigating the issue has gained substantial interest. Photocatalysts harness light energy for solar-to-chemical conversion reactions. The mechanism offers a promising solution for degrading harmful industrial dyes in wastewater.

The ZnO semiconductor is characterized by non-toxicity, wide bandgap, low cost, significant mobility and surface area, and favourable optical attributes, render it a preferred semiconductor in water treatment. The substance can be synthesised through various physical and chemical methods. A green and eco-friendly synthesis approach involving laser technology has also emerged. The technique absorbs photons to generate  $\bar{e}/h^+$  pairs, which participate in redox reactions and contaminant mineralisation.

The primary drawback of ZnO is a wide bandgap, limiting sunlight absorption to approximately 5%, resulting in photogenerated  $\bar{e}/h^+$  pairs recombination, reducing its effectiveness in dye photodegradation. Enhancing the solar harvesting power of ZnO via doping offers a solution. The structure, morphology, and photocatalytic attributes of ZnO affected by doping positively.

Employing laser technology might offers advantages over conventional methods, enabling efficient direct nanoparticle growth. In this study, Ce-doped ZnO 3D spherical nanoparticle catalysts were synthesised utilising two lasers: a 60-watt CW IRL and a 20-watt BL. The LACBS technique, which involves high temperatures and

rapid cooling, was also applied due to its doped NP yield potential. Furthermore, laser parameters, target composition, and liquid property adjustments allowed NP composition, inner structure, particle size distribution, and morphology regulation.

## **2.2 Dye pollutants**

Rising environmental pollution from inorganic contaminants, specifically water, arises from intensive industrialisation, posing risks to human health. Synthetic dyes are utilised in the tannery, paper, and textile industries. Wastewater from the industries is transported to water or other clean carrier media. Exposure to toxic pollutants can result in skin or eye irritation, liver, kidney, brain and central nervous system dysfunction, brain function illnesses, and neurological impairments. Moreover, the complex chemical structure of synthetic dyes, such as azo (MO, methylene blue, and Congo red), render them non-degradable. Consequently, identifying and removing the water contaminants are critical as their degradation products are carcinogenic and toxic to mammals and harmful to the environment [42].

### **2.2.1 The Methyl Orange (MO) dye**

Approximately 700,000 tonnes of dyes of over 10,000 types are industrially utilised as colouring agents, predominantly textiles. The MO is an azo dye with the  $C_{14}H_{14}N_3NaO_3S$  molecular formula. The synthetic dye records a maximum absorption peak of 464 nm and a 327.33 g molar mass. Applied as a weak acid-base indicator, MO dye is increasingly employed in printing, paper manufacturing, textile, plastics, cosmetics, pharmaceuticals and food industries [42][43].

Several health issues, such as skin diseases, vomiting and diarrhoea, have been associated with MO dye. Furthermore, the presence of the toxic pollutant in wastewater could result in skin and eye irritation, impaired liver, kidney, brain, central nervous system, and brain functions, and neurological disorders [39][44].

### **2.2.2 Dye removal techniques**

Several physical techniques, including adsorption, coagulation-flocculation, membrane filtration chemical, ion exchange, chemical precipitation, oxidation, and catalytic degradation, and biological approaches, such as microbial degradation, have been developed to eliminate toxic dyes from wastewater reservoirs. Nonetheless, adsorption was the most efficient method due to its simplicity and economic benefits. Dye molecules are adsorbed on adsorbent surfaces through hydrogen bonds and Van Der Waals interactions. Nanomaterials are excellent adsorbents as they possess considerable specific surface area and adsorption capacity, superior properties, and rapid adsorption equilibrium [34].

### **2.3 Metal oxide semiconductors for photodegradation**

Metal oxide semiconductors garnered attention in the 1950s, leading to a significant increase in the synthesis and investigation of inorganic oxide semiconductors. Among various oxides, noted that the wide ZnO semiconductor bandgap is ideal and technologically significant due to its extraordinary electronic, chemical, and optical characteristics [45].

At moderately high temperatures, metal oxides demonstrate excellent crystallinity and chemical and thermal stability and notable carrier mobility [46]. The substance is an amphoteric oxide, reacting with acids and bases to produce salt and water [47]. Metal oxides exhibit various functional properties, which substantially depend upon their crystal structure, morphology, composition, intrinsic defects, and doping. The functional attributes determine the synergistic combination of metal oxides, including significant area-to-volume ratio and tuneable optical, electrical, chemical, and catalytic attributes. Furthermore, the considerable chemical, structural, and environmental stability of metal oxides renders them applicable in emerging

applications, such as photocatalysts, catalysts, adsorbents, superconductors, semiconductors, ceramics, and antifungal agents [48][49].

Metal oxides can be prepared by directly heating metal elements with oxygen. Alternatively, the metal elements can be reacted with other chemicals. Numerous industrial techniques, such as chemical treatments of precursor reagents, hydrothermal and precipitation reactions, sol-gel, sputter-coating, and green synthesis, also produce metal oxides [47][49].

## 2.4 The fundamental properties of ZnO

The ZnO is a semiconductor commonly known as zinc white [5]. Commonly, the substance occurs in crystalline, which is almost insoluble in water and alcohol. Table 2.1 lists the most common fundamental attributes of ZnO. The hexagonal unit cell crystal has two lattice parameters, a and c [5]. The ZnO crystals also consist of multiple tetrahedral alternating  $O^{2-}$  and  $Zn^{2+}$  ion planes along the c-direction (see Figure 2.1). The surfaces can terminate with either  $Zn^{2+}$  or  $O^{2-}$ , leading to ZnO surfaces possessing positive or negative charges [49][50].

Table 2.1 The fundamental properties of ZnO semiconductor

Properties	Description/Value	Ref.
Unit cell structure	Hexagonal	[14]
Type of lattice	Wurtzite at 300 K=26.85°C	[14]
Sublattice	Hexagonal closed packed (hcp)	[14]
Molecular weight (g/mol)	81.40	[51]
Direct bandgap energy (eV)	~ 3.37	[31]
Excitation binding energy (meV)	60 at 300 K	[31]
Melting point (°C)	1975	[51]
Boiling point (°C)	2360	[51]
Lattice parameters (nm)	a = 0.325, c = 0.521	[14]
c/a ratio	1.602 (ideal value 1.633)	[14]

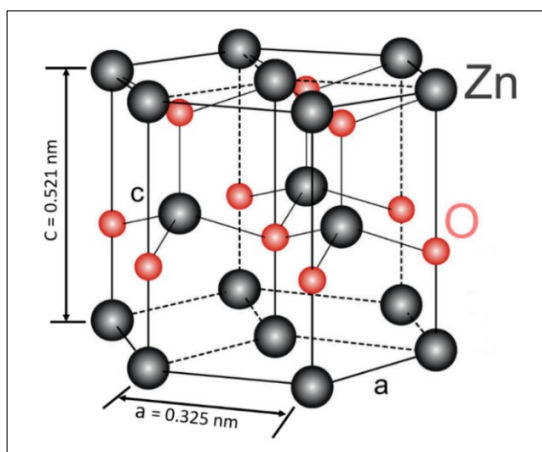


Figure 2.1 The hexagonal wurtzite structure of ZnO. (Note: Modified from [14])

Based on Figure 2.1, the ZnO structure comprises two interpenetrating hexagonal closely packed (hcp) sublattices. Each sublattice contains only one atom type, Zn or O, displacing each other along the threefold c-axis. The ZnO tetrahedral coordination results in its non-centrosymmetric structure. Meanwhile, the tetrahedral coordination of hexagonal ZnO wurtzite arises from each anion being surrounded by four cations [52].

The ZnO has demonstrated photocatalytic potential for environmental wastewater pollutant remediation from its considerable photosensitivity, non-toxicity, low cost, and environmental friendliness. Furthermore, ZnO can be crystallised in two predominant forms: wurtzite and zinc-blende under different conditions. Although ZnO can remove several organic contaminants in acidic and basic media, it suffers from rapid  $\bar{e}/h^+$  recombination. Consequently, modifying ZnO morphology has been attempted to elevate its photocatalytic activities [50][53].

#### 2.4.1 Optical properties of ZnO

The optical properties of semiconductor materials contribute to their intrinsic and extrinsic attributes. Intrinsic optical transition occurs between electrons in CB and holes in VB, producing  $\bar{e}/h^+$  exciton pairs from Coulomb interactions. Meanwhile,

extrinsic effects are related to dopants or defects, which typically result in discrete electronic states between the VB and CB [53].

The bandgap of ZnO is  $\sim 3.37$  eV leads to its ability to absorb a notable fraction of the short wavelength region. Various approaches have been applied to enhance ZnO photocatalytic efficiency. The techniques shift ZnO bandgap energy, creating intra-band levels, which effectively cause effective bandgap narrowing. The narrowed bandgap allows the absorption of longer wavelength. Consequently, the  $\bar{e}/h^+$  pair recombination rate is suppressed and increased charge separation efficiency [21][54].

#### **2.4.2 ZnO nanoparticles properties**

ZnO is widely employed in numerous areas, such as material science, agriculture, food, cosmetics, medicine, and diagnostics. Moreover, the substance is notably stable at high temperatures and pressures. The metal oxide can also be synthesised in the form of various nanostructures, including rods, flowers, tubes, and belts [55].

Nanotechnology refers to synthesising particles with sizes ranging between 0.1 nm and 100 nm, known as nanoparticles (NPs). NPs can be procured via different methods and formed into different shapes. Furthermore, the technology has been applied to produce NPs for varying purposes as it offers different approaches and significant control, considering the importance of nano-sized metal oxide particles. ZnO NPs have substantial surface-area-to-volume ratios and UV absorption capacity and unique physicochemical properties. As a nanomaterial, ZnO exhibits significant potential due to its distinctive catalytic and optical attributes, inexpensiveness, non-toxicity, and extensive applications in diverse areas [56]. Consequently, developing a reliable doped metal oxide NPs synthesis method is necessary [57].

## 2.5 ZnO NPs modification by doping

Fabricating visible-light active ZnO photocatalysts is among the primary challenges in semiconductor photocatalysis. Various techniques have been applied to enhance ZnO photocatalytic efficacy. Metal-doped ZnO photocatalysts exhibit elevated photoactivity, achieved through increased photo-induced charge carriers trapping sites. The phenomenon diminishes photoinduced  $\bar{e}/h^+$  pair recombination rates.

Several studies doped ZnO with transition metals [58][59] and rare earth RE metals [22][60] to procure photocatalysts with elevated photocatalytic activities (see Table 2.2). For instance, Malhotra was employed metal dopants, including Ce, Ag, Cu, and Al, to decrease the bandgap energy of photocatalysts utilised in varying pollutant degradation under visible light by shifting the bandgap energy, suppressing the recombination rate of electron-hole pairs, increasing charge separation efficiency. In [21]. Meanwhile, Damjan et al. (2022) obtained Ag-doped ZnO NPs with pulsed laser ablation in water. The report revealed that the photodegradation rate of methylene blue (MB) under UV irradiation with 0.32% Ag doped ZnO was the most efficient, almost twice the rate recorded by pure ZnO NPs [61].

Buzuayehu et al. (2023) synthesised 1% and 10% cobalt-doped from significantly pure nanosized composite substances through sol-gel self-combustion synthesis (SCS). The indirect bandgap reduction (redshift) from 3.22 to 2.70 eV indicated the optimal interstitial cobalt inclusion in the ZnO lattice. Furthermore, the XRD and TEM data validated the crystalline nature and nanoscale size range (20 nm–50 nm) of the materials. The carbon steel (CZ-Cs) also demonstrated superior catalytic reduction potential for MB within 12 min to ZnO under visible light [62].

Disinfecting Escherichia coli and pathogenic fungi of Fusarium gramine arum with 7% Cu-doped nanocrystalline ZnO was investigated by Ruichun et al. (2023). The Cu-ZnO exhibited enhanced disinfection properties within 5 h compared to undoped ZnO. The NPs were procured through facile one-pot solvothermal and were ~9 nm in size. The findings demonstrated a promising green alternative and visible light excitation catalyst method of eliminating bacteria and agricultural pathogenic fungi from wastewater [63].

Table 2.2 A summary of selected recent reports doping ZnO by variety of metal dopants for efficient photocatalyst in the degradation of different pollutant.

Metal type	Dopant	Fabrication method	Substrates	Bandgap (eV)	Target pollutant	Photodegradation rate, light and time	Size (nm)	Optimal catalyst concentration	Ref.
Rare Earth Metals	Ce	sol-gel	Zn(NO <sub>3</sub> ) <sub>2</sub> ·6H <sub>2</sub> O Ce(NO <sub>3</sub> ) <sub>3</sub> ·6H <sub>2</sub> O	2.98	RhB	96.67%, Visible, 90min	44.9	1 wt%	[64]
	Dy	tartaric acid-assisted combustion	Zn(NO <sub>3</sub> ) <sub>2</sub> ·6H <sub>2</sub> O Dy(NO <sub>3</sub> ) <sub>3</sub> ·6H <sub>2</sub> O	-	MB	97%, Visible, 75min	15	5 wt. %	[65]
	Eu	Co-precipitation	Zn(NO <sub>3</sub> ) <sub>2</sub> ·6H <sub>2</sub> O Eu(NO <sub>3</sub> ) <sub>3</sub> ·5H <sub>2</sub> O	3.28	MB	97.2%, UV, 60min	45	0.09	[66]
	Gd	Supercritical antisolvent (SAS) precipitation	ZnC <sub>4</sub> H <sub>6</sub> O <sub>4</sub> Gd(CH <sub>3</sub> CO <sub>2</sub> ) <sub>3</sub> ·H <sub>2</sub> O	3.05	AZ	Visible, 180min	19	0.7 mol% (80/1 :w/w :Zn/Gd)	[67]
	Ho	sol-gel	Zn(NO <sub>3</sub> ) <sub>2</sub> ·6H <sub>2</sub> O Ho(NO <sub>3</sub> ) <sub>3</sub> ·5H <sub>2</sub> O	3.10	RhB	95.7%, UV, 240min	12.7	0.03	[68]
	Tb	solvothermal	-	-	-	RhB, UV, 40min	19.34	0.03	[69]
Transition Metals	Al	chemical vapor deposition	Zn powder Al metals	3.27	MB	61.86%, UV, 180min	72.5	0.08	[70]
	Au	simple heat treatment	Zn(NO <sub>3</sub> ) <sub>2</sub> ·6H <sub>2</sub> O Au-gold	3.024	MO	99%, UV, 150min	32.53	1.0%	[71]
	Ni	sol-gel	Zn(NO <sub>3</sub> ) <sub>2</sub> ·6H <sub>2</sub> O NiCl <sub>2</sub> ·6H <sub>2</sub> O	3.03	MO	94%, Sunlight, 80min	25.34	0.04	[72]
	Fe	Supercritical antisolvent (SAS) precipitation	C <sub>4</sub> H <sub>6</sub> O <sub>4</sub> Zn·2H <sub>2</sub> O FeCl <sub>3</sub> ·6H <sub>2</sub> O	2.83	AO7	52%, Visible, 180min	19	0.75mol%	[73]
	Y	precipitation under ambient pressure	Zn(NO <sub>3</sub> ) <sub>2</sub> ·6H <sub>2</sub> O Y(NO <sub>3</sub> ) <sub>3</sub> ·6H <sub>2</sub> O	3.21	carbaryl	sunlight >UV, 30min	46.69	2 mol. %	[74]

## 2.6 Rare earth metal modification

Rare earth (RE) metals have several distinctive characteristics. RE metals readily combine with functional groups of organic dyes due to their 4f and 4d vacant orbital electronic structures, advantageous for doping semiconductor metal oxides

[75]. RE-doped ZnO NPs can be an excellent catalyst and promote the photocatalytic activity of organic compounds by contributing to concentrating the organic pollutants on their surfaces. Moreover, Ce-doped ZnO NPs might be an effective photocatalyst by reducing its bandgap, achieved through extra energy level creations for solar light utilization [17][75][76].

Doping with RE metal ions can effectively elevate semiconductor photocatalytic ability by improving adsorption capacity. The modification also shifts the absorbance of semiconductors to the visible region, enhancing the photocatalytic activity of the host material [39]. For instance, the RE - Ce<sup>3+</sup> ions are readily integrated into ZnO wurtzite structures without becoming impurities, narrowing its bandgap, and enabling the doped material to utilise the visible region of sunlight [39].

Ce dopants have also recorded positive effects on ZnO photocatalytic activities. Consequently, manufacturing Ce doped ZnO nanostructure with different morphologies is attracting significant interest worldwide. Nonetheless, only a few reports are available on elevating ZnO photocatalytic efficiency with Ce utilizing high power and CW laser, as in the present study. Choudhary et al. (2023) fabricated nanowires from Ce-doped ZnO through thermal decomposition route with outstanding photodegradation performance. Optimal photocatalyst bandgap was 3.17 eV for MB, MG, MO and RhB dyes photo-decolorization at 96.6%, 92.2%, 67.1% and 77.7% photodecomposition efficiencies, respectively of solar light exposure. Repeatability reusability experiments give an idea of the outstanding come with stability of synthesized nanowires for wastewater treatment applications [77].

Hajer et al. (2021) prepared RE ion Er-modified ZnO NPs and assessed their application in degrading RR180 azo dye molecules. The doped crystallite size calculated according to the Debye Scherrer formula indicated reduction, recording an

optimal concentration of 3 wt.% Er. The results indicated that the RE/ZnO were more efficient than pure ZnO. Under visible light irradiation, the NPs achieved 99% degradation after 45 min with increasing Er concentration up to 3 wt.% [78].

The photocatalytic activity of 3% La-doped ZnO nanotubes was evaluated by Soares et al. (2024). The report employed the methylene blue (MB) and Ciprofloxacin (CIP), which were degraded under UV irradiation. The basic and alkaline pH values (8-12) utilised decreased the crystallite size of the nanomaterial, which might have contributed to the varying bandgap energy values. The nanorods also appeared to be formed from mesopores. The La-doped ZnO nanotubes were synthesised via coprecipitation and removed MB (91.45 %) and CIP (87.6 %) more rapidly in typical pseudo-first-order kinetics within 150 min. The study also noted that the Y/ZnO had superior stability and reusability after three consecutive uses [79].

Petronela et al. (2023) investigated the effects of 0.05%, 0.1%, 0.5%, and 1% Nd doping on ZnO photocatalytic MB and CIP drug pollutants degradation with visible light irradiation. The photocatalysts were procured through electrospinning–calcination. Based on the findings, the reaction rate constant increment was almost linear with the mean crystallite size. Nevertheless, the mean crystallite size varied between 24.2 nm and 42.1 nm. Subsequently, the ideal catalyst, 0.1% Nd-doped ZnO, was employed to optimise CIP and MB photodegradation. After 120 min, the removal efficiency was approximately 100%, with  $5.291 \times 10^{-2} \text{ min}^{-1}$  (CIP) and  $4.780 \times 10^{-2} \text{ min}^{-1}$  (MB) rate constants ( $k$ ) under the established optimal parameters. The elevated photocatalytic properties were due to the electron scavenging characteristic of Nd ions, preventing  $\bar{e}/h^+$  pair recombination [80].

Anamika et al. (2023) suggested incorporating  $\text{Sm}^{3+}$  into the ZnO through a green synthesis technique. The NPs crystallite size decreased with increasing  $\text{Sm}^{3+}$  ion

concentration as the ions inhibits NPs growth. The  $\bar{e}/h^+$  pair recombination rates were also diminished with rising  $\text{Sm}^{3+}$  ion wt%. According to the findings, the 10 wt%  $\text{Sm}^{3+}$  doped ZnO NPs recorded optimal photodegradation efficiency towards methyl green dye under UV irradiation for 50 min. The doped photocatalyst achieved a 91% dye degradation rate compared to the 26% documented by pristine ZnO NPs. The core-shell heterostructure nano junctions formed between  $\text{Sm}_2\text{O}_3$  and ZnO contributed to the elevated photocatalytic performance [81].

Overall, metal dopants positively influence ZnO photocatalysis of various organic pollutant degradation. For instance, RE dopants delay  $\bar{e}/h^+$  recombination reactions by introducing impurities that act as  $e_{cb}^-$  traps, enhancing photoactivity. Incorporating impure energy levels in the bandgap also raised the absorption of ZnO to higher wavelengths. The phenomenon is due to the perturbation in the energy levels of the host crystal. Furthermore, several new energy levels are formed under the CB of the host matrix. Doping RE ions also add effective organic pollutant-adsorbing ability as they can form complexes on catalyst surfaces. Although metal oxide NPs with RE might enable a wide wavelength range and physical properties, reports on utilising RE ions on ZnO photocatalysis are limited [82]. Specifically, the information might present solutions regarding  $\bar{e}/h^+$  pair recombination and the lack of solar light utilisation.

## **2.7 The fundamental properties of Ce (Cerium) metal**

Cerium is a unique among rare earth elements owing ability to exist in multiple oxidation states, combined with its high reactivity with oxygen, makes cerium exceptionally valuable in chemical reactions [83]. Cerium seems to be one of the most suitable candidates for enhancing the photocatalytic properties system due to it has very special physical electronic properties, like availability of 4f orbital, and ionic

bonding between Ce–O, chemically stable nature. Ce metal is an excellent impurity in catalytic application due to ionic properties of facile redox chemistry coupling of  $Ce^{3+}/Ce^{4+}$  at nanoscale. Easy formation of labile oxygen vacancies with relatively high mobility of bulk oxygen species depending on the morphological structure of the host [84][85][86]. The recorded  $Ce^{4+}$  (0.092 nm) and  $Ce^{3+}$  (0.1034 nm) radii, which were notably larger than  $Zn^{2+}$  (0.074 nm) [87][88]. Table 2.3 lists of the most common fundamental attributes of Ce metal.

Table 2.3 The fundamental properties of Cerium metal.

Properties	Description/Value	Reference
Atomic Number	58	[89]
Atomic weight (g/mol)	140.12	
Melting point (°C)	795	
Boiling point (°C)	3430	
Density (gm/cm <sup>3</sup> )	6.77	
Electron Configuration	4f <sup>1</sup> 5d <sup>1</sup> 6s <sup>2</sup>	

Ce metal can easily trap photogenerated electrons during charge transfer from metal oxide CB, reducing  $\bar{e}/h^+$  pair recombination rates and enhancing photocatalytic activity mainly involved in the reactions leading to the elimination of organic pollutants in wastewater [76][86]. In addition, Cerium can be effectively used as photocatalyst by tuning its band gap due to creation of extra energy levels in the host bandgap. Therefore, simultaneous surface modification and doping not only changes the surface morphology, size and surface charges of the nanoparticles synthesized, but also significantly shifts the band gap energy to the visible region, where utilization of solar light is more comparable to that of the UV region [17].

## 2.8 The fundamental properties of photocatalyst

Photocatalysts are materials that accelerate chemical reactions using light energy by generating electron-hole pairs. These materials have outstanding physicochemical, electronic, and structural properties that enhance their performance

in the applications stated. The process of transforming solar or light energy into chemical energy is known as photocatalysis by acceleration of chemical transformation with the presence of light and catalyst, helps to degrade harmful contaminants in aqueous solution by breaking them down [90].

Their effectiveness depends on several fundamental properties and operational factors [90][91]:

1. **Bandgap Energy:** A suitable bandgap ( $E_g$ ) allows activation by wavelength (Visible or UV or combination of both) light and photoexcited electrons are promoted from the valence band to the conduction band, to produce electron-hole pairs and enable redox reactions: via hydroxyl radicals  $OH^\bullet$ .
2. **Surface Area Characteristics:** Larger areas provide more active sites for reactant adsorption and radical generation, NPs catalysts reducing electron-hole recombination.
3. **Morphology:** Particle size and shape influence light absorption and charge transfer efficiency.
4. **Chemical Stability:** Must resist corrosion

Factors Influencing Photocatalytic Efficiency are pH, Temperature, Light Intensity, Pollutant Concentration, Catalyst Loading. The factors which are responsible for good photocatalytic process are low recombination and life time charge separation, physiochemical stability, low cost, high adsorption surface area, and high light absorption efficiency [47][90][92].

## **2.9 Advanced Oxidation Process of pollutant degradation**

Advanced oxidation processes (AOPs) a set of chemical reactions to remove organic materials in water, are gaining interest as an alternative solution in wastewater treatment due to their ability to eliminate different hazardous environmental pollutants.

Photocatalysts are essential elements in AOPs. Chaker et al. (2021) also noted that photocatalytic oxidations offer low-cost removal methods of significant efficiency [93]. Moreover, AOPs exhibit a rapid degradation rate and possess the ability to mineralise organic compounds to green products, operate under ambient temperature and pressure, and reduce the toxicity of organic compounds [94]. The green or by-products formed from oxide–water interactions, such as ROS and leached metal ions, which influence MO degradation trajectories. These species can enhance or alter photocatalytic efficiency and intermediate formation [49][93].

AOP mechanisms are categorised as homogeneous and heterogeneous photocatalysis. Heterogeneous photocatalysis employs semiconductor oxide photocatalysts, where the catalysts are in a different phase from the reactants [47][95]. The photocatalyst can utilise UV and solar radiation [49]. In aqueous solutions, heterogeneous photocatalytic activities occur at the solid-liquid interface. Wazir (2015) indicated that the process comprises three independent steps [96]:

- (i) the transfer of pollutants to the catalyst surfaces,
- (ii) adsorption of the pollutants on the surfaces,
- (iii) upon absorption of a photon, reactive  $OH^{\bullet}$  radicals are generated on the photocatalyst surfaces, degrading organic pollutants and mineralising them.

Photocatalysis accelerates photoreactions in the presence of catalysts. During the reactions, light is absorbed by a substrate typically adsorbed on solid catalysts. In principle, photocatalysis can be summarised in three phases as illustrated in Figure 2.2. The first stage involves the generation of charge carriers through  $\bar{e}$  excitation. Subsequently, charge carriers migrate. Finally, surface reactions occur.

Photocatalytic activity relies upon the ability of catalysts to form free radicals that can undergo secondary reactions. Consequently, a photocatalyst is defined as a

material that can absorb light energy equal to or over the bandgap energy of a semiconductor. The energy is then employed to produce  $\bar{e}/h^+$  pairs on its surfaces, enabling chemical transformations of the reactants [47].

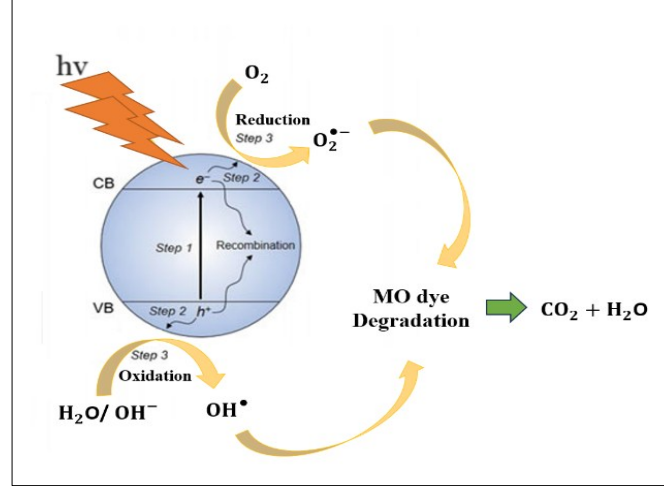
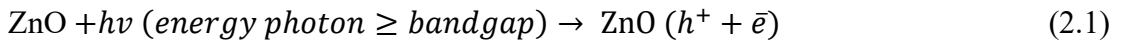


Figure 2.2 The schematic presentation of the photocatalytic mechanism and degradation process

Photogenerated  $h^+$  formed in the VB can oxidise  $H_2O$  from an aquatic environment to  $OH^\bullet$ , which is responsible for oxidation. Meanwhile, the  $\bar{e}$  formed in CB will be adsorbed by  $O_2$  to produce superoxide radical ions ( $O_2^{\bullet -}$ ), contributing to reduction. The radicals ROS might interact with pollutants and mineralise them into by-products  $CO_2$  and  $H_2O$  [49][93][97]. Equations (2.1) – (2.8) represent the activation of photocatalysts by light energy:



The reduction and oxidation processes are shown according to the following equations:

